

Identifying non-stationary groundwater level response to North Atlantic ocean-atmosphere teleconnection patterns using wavelet coherence

Ian Paul Holman¹, Monica Rivas-Casado¹, John P. Bloomfield² & Jason J. Gurdak³

¹Department of Environmental Science and Technology, Cranfield University, Bedford MK43 0AL, Cranfield, UK

²British Geological Survey, Maclean Building, Crowmarsh Gifford, Wallingford, Oxfordshire, OX10 8BB, UK

³Department of Geosciences, San Francisco State University, 1600 Holloway Ave., San Francisco, CA 94132, USA

Abstract The first comprehensive use of wavelet methods to identify non-stationary time-frequency relations between North Atlantic ocean-atmosphere teleconnection patterns and groundwater levels is described. Long-term hydrogeological time series from three boreholes within different aquifers across the UK are analysed to identify statistically significant wavelet coherence between the North Atlantic Oscillation, East Atlantic pattern, and the Scandinavia pattern and monthly groundwater-level time series. Wavelet coherence measures the cross-correlation of two time series as a function of frequency, and can be interpreted as a correlation coefficient value. Results not only indicate that there are common statistically significant periods of multiannual-to-decadal wavelet coherence between the three teleconnection indices and groundwater levels in each of the boreholes, but they also show that there are periods when groundwater levels at individual boreholes show distinctly different patterns of significant wavelet coherence with respect to the teleconnection indices. The analyses presented demonstrate the value of wavelet methods in identifying the synchronization of groundwater-level dynamics by non-stationary climate variability on time scales that range from interannual to decadal or longer.

Introduction

Effective water resource management requires an understanding of the effects of natural climate variability on recharge and groundwater levels, particularly in the context of increasing climate uncertainty. The soil, unsaturated, and saturated zones of aquifers can filter or remove much of the high-frequency signals and noise (Dickinson et al. 2004), producing a buffering effect which provides resilience to water resources and associated ecosystems under short-term climate extremes. However, recent studies (Hanson et al. 2004; 2006; Gurdak et al. 2007; Holman et al. 2009) have indicated that groundwater-level fluctuations are affected by relatively low frequency (interannual to multidecadal) atmospheric and ocean circulation systems such as the North Atlantic Oscillation (NAO), which are known to affect weather and river flows (Jones and Banner 2003; Qian and Saunders 2003; Barker et al. 2004; Schroder and Rosbjerg 2004; Hannaford and Marsh 2008). Milly et al. (2008) assert that stationarity should no longer serve as the central assumption in water resource risk assessment and planning largely because of climate change and natural low-frequency climate variability such as from the NAO, Pacific Decadal Oscillation (PDO; Mantua and Hare 2002), or Atlantic Multidecadal Oscillation (AMO; Enfield et al. 2001).

However, little is known about the coupling between global climate oscillations and hydrogeological systems (Gurdak et al. 2009), which is important given the lack of skill of existing climate models to adequately represent large-scale climate features. For example, 15 of the 18 global, coupled general circulation models that were used in phase 2 of the Coupled Model Intercomparison Project (CMIP2) were able to simulate the NAO pressure dipole but were deficient in capturing observed decadal variability (Stephenson et al. 2006). Stephenson et al. (2006) concludes that the models' inability to capture the observed decadal variability in NAO might signify a deficiency in their ability to simulate the NAO-related responses to climate change, which would have implications for the confidence in climate-impact studies, and further strengthen the need for adaptive groundwater management strategies that incorporate knowledge of interannual-to-multidecadal climate variability. Previous studies have inferred relations between low-frequency climate signals and groundwater levels using spectral analysis (Gurdak et al. 2007; Luque-Espinar et al. 2008; Holman et al. 2009). Although methods such as singular spectrum analysis can detect nonlinear oscillations in noisy time series (Ghil

et al. 2002), most spectral analysis methods assume that the underlying processes are stationary in time with continuous, homogeneous (i.e. constant), and periodic waves up to infinity (Boggess and Narcowich 2001). Many geophysical time series such as those generated by climate and hydrologic variables, are stochastic and non-stationary in their behaviour, presenting many time and frequency scales of variation (Grinsted et al. 2004; Maraun and Kurths 2004), requiring methods that can identify localized intermittent periodicities (Boggess and Narcowich 2001). Thus, appropriate analytical methods are needed for hydrogeological time-series analysis to account for nonstationarity in hydroclimatic processes.

In this technical note, we describe the first comprehensive use of wavelet methods (Grinsted et al. 2004) to analyse hydrogeological time series in order to identify statistically significant wavelet coherence between North Atlantic teleconnection indices and monthly groundwater level time series in three boreholes within different aquifers across the UK.

Material and methods

Study sites

Three boreholes, located at Ampney Crucis, New Red Lion, and Dalton Holme (Fig. 1) were selected along a northeast–southwest transect across England, spanning two major aquifer complexes and the width of the country. The sites are part of the UK national borehole observation network (Marsh and Hannaford 2008) and are all known to be unaffected by abstraction and to fully penetrate the active aquifers at each site. The Ampney Crucis and New Red Lion boreholes are located in the Jurassic Limestone aquifer. Water levels at Ampney Crucis are confined, while those at New Red Lion are confined at high water levels and unconfined at low water levels. The Jurassic Limestone aquifer consists of thin limestones (the main aquifer units), interlayered with sandstones, ironstones, sandy-shales and shales (Allen et al. 1997). The third borehole, at Dalton Holme, is located in the unconfined Chalk aquifer beneath about 6 m of glacial till. The Chalk is the major aquifer in the UK and is a thick fractured dual porosity limestone (Price 1993; Allen et al. 1997). Flow in both the Jurassic Limestone and Chalk aquifers is dominated by fracture flow, and they are both characterised by high transmissivities (T) and low storage coefficients (S).

Monthly groundwater levels at each site are shown in Fig. 2, and Table 1 summarises features of the groundwater hydrographs. Depth to groundwater at all three sites varies between about 10 and 20 m (Table 1). The hydrographs all show strong annual fluctuations between about 5 and 20 m (consistent with high transmissivity and low storage coefficient fractured limestone aquifers), and show more prolonged periods of low or high groundwater level stands in response to changes in multi-seasonal trends in rainfall and recharge. Like many groundwater hydrographs, even when seasonality is removed from the signal, autocorrelations in groundwater levels of between 6 and 12 months (Table 1) are observed—the Pearson correlation co-efficient has been used to calculate autocorrelation at successive lags, and autocorrelations are taken to be significant at confidence levels of 95% or better. Average annual rainfall is similar at all three sites, being 587, 760 and 678 mm for Ampney Crucis, New Red Lion, and Dalton Holme, respectively.

Climate index data

Data for three large North Atlantic teleconnection patterns (Fig. 2) have been used:

- North Atlantic Oscillation (NAO): The leading pattern of atmospheric variability in the North Atlantic region, influencing the intensity and location of the North Atlantic jet stream and storm tracks that bring much precipitation to Europe, is defined as the difference between the normalized sea-level pressures over Gibraltar and SW Iceland. Strong positive phases, when a strong low pressure is centred near Iceland and a strong high pressure is located over the middle of the North Atlantic Ocean, tend to be associated with above-average precipitation over northern Europe in winter, whereas Northern Europe in winter is cold and dry when the pressure centres are weaker (negative phase). Monthly data from the Climatic Research Unit are available from 1823 to 2009 (CRU 2010; Jones et al. 1997). The NAO exhibits considerable interseasonal and

interannual variability, and the wintertime NAO also exhibits significant multi-decadal variability (Hurrell 1995). For example, the negative phase of the NAO dominated the circulation from the mid-1950s through the 1978/1979 winter. An abrupt transition to recurring positive phases of the NAO occurred during the 1979/1980 winter, with the atmosphere remaining locked into this mode through to the 1994/1995 winter season, after which there was a return to the strong negative phase of the NAO.

- East Atlantic (EA) pattern: The second most prominent mode of low-frequency variability over the North Atlantic, derived from rotated principal component analysis (RCPA) of monthly mean standardized 500 mbar geopotential height anomalies (CPC 2010). The positive phase is associated with above-average temperatures and precipitation over northern Europe. Monthly data from 1950 to 2010 are available from the National Oceanic and Atmospheric Administration's Climate Prediction Centre (CPC 2010). The EA pattern exhibits very strong multi-decadal variability in the time series record, with the negative phase prevailing during much of 1950–1976, and the positive phase occurring during much of 1977–present. The positive phase of the EA pattern was particularly strong and persistent during 1997–2004.
- Scandinavia pattern: Derived from a similar methodology to the EA pattern, the positive phase of the Scandinavia pattern is associated with below-average temperatures across Western Europe and with above and below-average precipitation across Central Europe and Scandinavia, respectively. It has been linked to wet UK Autumns (Blackburn and Hoskins 2001). Monthly data from 1950 to 2010 are available from the CPC (CPC 2010). The time series for the Scandinavia pattern exhibits relatively large interseasonal, interannual and interdecadal variability. For example, a negative phase of the pattern dominated the circulation from early 1964 through mid-1968 and from mid-1986 through early 1993. Negative phases of the pattern have also been prominent during winter 1988/1989, spring 1990, and winter/spring 1991/1992. In contrast, positive phases of the pattern were observed during much of 1972, 1976 and 1984.

An introduction to wavelet analysis

Wavelet methods are a multi-resolution analysis used to obtain time-frequency representations of a continuous signal. They have the advantage over other methods (e.g. Fourier analysis) of being designed to model signals that have localized time features. The objective of the analysis is to decompose a signal, expressed as a function of the time variable t , into various frequency components using building blocks (Bogges and Narcowich 2001). In wavelet analysis these building blocks are defined by wavelets. A wavelet is a small “wave” that travels for one or more periods and can be translated forward or backward in time, as well as stretched and compressed by scaling, to identify low- and high-frequency periods within the signal. Once a wavelet is constructed, it can be used to filter or compress signals. In contrast, the building blocks in Fourier analysis, for example, are infinite periodic combinations of sine and cosine functions that vibrate at a frequency of n times per 2π interval. A description of wavelet methods can be found in Meyer (1993), Nason (2008), Walnut (2002) or Grinsted et al. (2004), and are briefly described in the following.

A wavelet is defined by a function $\psi_0(\eta)$, where η is a non-dimensional time parameter, that has zero mean and is localised in both time and frequency space (Farge 1992; Percival and Walden 2000). For these assumptions to be satisfied, the function needs to have the following basic properties: the integral of $\psi_0(\eta)$ is 0, $\int_{-\infty}^{\infty} \psi_0(\eta) \delta\eta = 0$, and the square of $\psi_0(\eta)$ integrates to unity, $\int_{-\infty}^{\infty} \psi_0^2(\eta) \delta\eta = 1$. If the second equation holds, then the function is non-zero only over a finite interval (Bogges and Narcowich 2001; Fig. 3). There are a set of pre-defined and commonly used wavelets designed to have these basic properties (Carmona et al. 1998). Some examples are the Cauchy, Morlet, Difference of Gaussian (DOG) and the Haar wavelets.

Wavelets are used to decompose a given signal into a sum of translation and scaling of a selected wavelet function (Bogges and Narcowich 2001). The selected wavelet used for the decomposition is commonly known as the mother wavelet function. The mother wavelet is shifted forward and backward in time, along the localized time index η , to filter or compress signals. This process is repeated for low and high frequency wavelets by varying the wavelet scale (i.e. stretching and

compressing the wavelet). The wavelet is normalized to have unit energy at all times (Grinsted et al. 2004). The convolution with a scaled and normalized mother wavelet of a time series ($x_n, n=1, \dots, N$) with uniform time steps δt is known as the continuous wavelet transform (CWT).

In contrast to the CWT which assesses the periodicities and phases of cycles within a single dataset, the cross wavelet transform (XWT) identifies the cross wavelet power of two time series, in this case a teleconnection index and a groundwater level record. For two given time series, ($x_n, n=1, \dots, N$) and y_n ($n=1, \dots, N$), the XWT W_n^{XY} is calculated as:

$$W_n^{XY}(s) = W_n^X(s)W_n^{Y*}(s) \quad (1)$$

Where $W_n^X(s)$ is the CWT of time series x_n and $W_n^{Y*}(s)$ is the complex conjugate of $W_n^Y(s)$, the CWT of time series y_n .

When written in the polar form, the cross wavelet spectrum can be decomposed into the amplitude or crosswavelet power $|W_n^{XY}(s)|$ and the phase $\phi_n(s)$ (which indicates the delay between the two signals at time t and scale s) as follows:

$$W_n^{XY}(s) = |W_n^{XY}(s)|e^{n\phi_n(s)} \quad (2)$$

The cross wavelet spectrum, although very useful to detect the phase spectrum, can potentially lead to misleading results as it is just the product of two non-normalized wavelet spectrums (Maraun and Kurths 2004). This can lead to significant cross wavelet spectrum being identified even when there is no relationship between the two time series. The wavelet coherence (WTC) avoids this problem by normalizing to the single wavelet power spectrum and is calculated as follows:

$$WCT = \frac{|W_n^{XY}(s)|}{[W_n^X(s)W_n^{Y*}(s)]^{0.5}} \quad (3)$$

where the notation corresponds to that in Eq. 1.

The WTC ranges from 0 to 1 and measures the cross-correlation of two time series as a function of frequency (Torrence and Compo 1997), i.e. local correlation between the time series in time-frequency space. It can be interpreted as a correlation coefficient; the closer the value is to 1 the more correlated are the two series. Statistically significant wavelet coherences were identified using a point-wise test. The test is implemented using Monte Carlo methods (Grinsted et al. 2004). A total of 1,000 realizations with the same first-order autoregressive (AR1) process coefficients as the two input data sets are generated using Monte Carlo techniques. The wavelet coherence is then calculated for each of these realizations and the significance level is calculated for each scale.

The power spectrum always has some degree of error at the beginning and end of the analysed signal because of the finite-length of the underlying data. Torrence and Compo (1997) propose the calculation of a cone of influence (COI) which determines the region of the wavelet spectrum where these edge effects need to be excluded.

Methodology

The analysis has been carried out in MATLAB using the script developed by Grinsted et al. (2004), which can be downloaded from Grinsted et al. (2011). The methodology has been divided into the three main steps described in the following:

Step 1. Detection of outliers: time series were scanned for outliers using descriptive statistics and box-plots.

Step 2. Wavelet analysis for a single time series: the CWT was estimated for each of the groundwater series, as well as the selected North Atlantic teleconnection indices. In this study, we have used the

Morlet wavelet (Eq. 4; Fig. 3) because it provides a good balance between time and frequency localization (Grinsted et al. 2004).

$$\psi_0(\eta) = \pi^{1/4} e^{i\omega_0\eta} e^{-1/2\eta^2} \quad (4)$$

where ψ_0 is the wavelet function, e represents exponential, ω_0 is the dimensionless frequency and η is the dimensionless time. In this study $\omega_0=6$. The power spectrum was calculated for frequency bands from 2 months up to 32 years. Each band occupies a bandwidth that is twice as wide as the previous band and half as wide as the next one. The spectrum was then estimated for a total of twelve sub-frequencies within each band. Plots of CWTs were visually inspected to identify those years where areas of high (>0.5) wavelet spectrum were present.

Step 3. Wavelet analysis of two autocorrelated time series: the cross wavelet spectrum and the wavelet coherence were estimated for the combinations of time series of groundwater levels and North Atlantic teleconnection indices. The spectrums were estimated for the same frequency bands and sub-bands as those used for the CWT. The COI of the CWT, the XWT and the WTC has been set to identify those wavelet power spectrums that have a drop of e^{-2} of the value at the edge (Torrence and Compo 1997). The relative lag between time series was inspected using the phase arrows. Arrows pointing right indicate that the two time series are in phase. Arrows pointing left show when the time series are in anti-phase and arrows pointing down or up show that one time series is leading the other by 90° .

Results

Although the methodological steps described previously (CWT on individual time series, XWT between pairs of time series and wavelet coherence on the XWT to identify statistically significant relationships between pairs) were necessarily followed, we focus our presentation of results and discussion on the wavelet coherence which provides the robust outcomes of interest to the reader, although the CWT are shown in Fig. 4 for the 6 time series. As described in the previous, there are three main elements within WTC plots (Fig. 5):

1. The times and periodicities of statistically significant wavelet coherences at the 5% significance level, as indicated by the areas within the bold black lines.
2. The phase relationship between the spectra which is portrayed by the direction of the arrows.
3. The COI showing the (paler shaded) region of the wavelet spectrum where edge effects due to the finite length nature of the underlying data cannot be ignored.

Figure 5 shows that the distribution of significant coherence is relatively consistent for a given pattern across all three borehole sites, which is consistent with the regional influence of these large-scale patterns—for example, periodicities of around 2.6 and 5 years are observed with the Scandinavia Pattern and the NAO, respectively, at the three boreholes. However, at a given site, the distribution of significant coherence in time and periodicity varies fundamentally between the three teleconnection indices, as might be expected from the differing dynamic behaviours of the indices (Figs. 2 and 4) and the likely sensitivities of the boreholes to the propagation of the climate signal to the groundwater levels due to their different geographical locations (with respect to relative proximity to continental Europe and the Atlantic Ocean) and hydrogeological systems (confined to unconfined).

Figure 5 therefore shows that there are common statistically significant episodes of multiannual-to-decadal wavelet coherence between the three teleconnection indices and groundwater levels in three different boreholes (and different aquifers), but also that there are periods where groundwater levels at individual boreholes show distinctly different patterns of significant wavelet coherence with respect to the teleconnection indices. For example, Fig. 5 shows that:

- There are statistically significant episodes of wavelet coherence at multiannual periodicities of around 2.5, 3, 5, 10.5 and 19 years that are common across the three boreholes (with the exception of the 19-year periodicity for which the New Red Lion record is too short).
- The timing of the statistically significant episodes of wavelet coherence differs between the boreholes. For example, the Scandinavia Pattern coherence with an approximately 2.5-year periodicity lasts until around 1970 in New Red Lion and Ampney Crucis but extends to 1975 in Dalton Holme; whilst the coherence with an approximately ~3.5 year periodicity starts in 1995 in New Red Lion and Dalton Holme, but not at Ampney Crucis. Similarly, the significant wavelet coherence at Ampney Crucis with NAO at about 5 years between 1975 and 1992 is not observed at either of the other two sites at this time, but appears to occur from about 1992 onwards.
- Most of the statistically significant wavelet coherence are in-phase (arrows pointing to the right), with the exception of the Scandinavia Pattern periodicity at around 3.5 years and the North Atlantic Oscillation periodicity at around 19 years.
- There is evidence of phase differences in the wavelet coherence between the teleconnection indices and the groundwater levels in the boreholes. For example, at the 1-year periodicity (i.e. annual recharge), the arrows indicating the phase difference are mostly horizontal at Ampney Crucis indicating an in-phase relationship between the groundwater level and the teleconnection indices, which is consistent with rapid recharge due to the shallower and fractured nature of the unsaturated zone. In contrast, the arrows have a greater vertical component at Dalton Holme, indicating a greater lag between the groundwater level and the teleconnection indices. This is consistent with the longer autocorrelation in Table 1, slower recharge through the unsaturated zone of the chalk and the borehole's location away from the aquifer outcrop.

As would be expected, there is little consistent wavelet coherence apparent at any of the boreholes for periodicities of less than 1 year, demonstrating that these large-scale teleconnection indices are not the drivers of short term (seasonal) variability in groundwater level dynamics, which are driven by local patterns of precipitation and evapotranspiration.

Discussion and conclusions

The previous use of wavelet methods in understanding groundwater dynamics has been limited—for example, Slimani et al. (2009) used CWT on groundwater levels but did not test for significance, whilst Henderson et al. (2009) used CWT and XWT to identify sub-daily to daily tidal pumping of submarine groundwater. This is the first such study of groundwater dynamics to use both cross wavelet spectrum and wavelet coherence to assess the non-stationary relationships between climatic indices and groundwater level oscillations. Figure 5 demonstrates that the methods provide initial evidence for both common responses in groundwater levels across aquifer types and different regions of the UK to large-scale climate oscillations such as the NAO.

The wavelet coherence in Fig. 5 also shows that non-stationary responses in groundwater levels to climate variability are apparent, such that the wavelet coherence at a particular periodicity for any one teleconnection index is variable, with periods of statistically significant coherence being followed by periods of low coherence. This may relate to the observed variability in the indices—for example, the winter NAO was mostly high during the first three decades of the twentieth century, followed by a period of variable but generally low index values until the 1970s, after which the index increased to the high values measured in the early 1990s (Osborn 2006). Alternatively, or in addition, the variability in coherence may relate to the individual climate oscillations of different periodicities within the indices combining to form constructive and destructive interference patterns, a process that was suggested by Hanson et al. (2004) and Holman et al. (2009). However, further wavelet methodological development is required to enable wavelet analysis techniques to quantify the way in

which different periodicities within the climate oscillations combine in order to improve our understanding of long-term controls on aquifer system function.

The relation between low-frequency climatic signals and groundwater levels will be complex, given the lags introduced to the lower frequency signals as they pass through the soil zone and through the unsaturated and saturated zones of aquifers (Gurdak et al. 2007). The filtering and lagging of climate signals, indicated by the differential directions of the vectors for a given periodicity between the boreholes within the wavelet coherence plots, might be expected to be a function of hydrogeological factors such as the hydraulic characteristics of the soil zone and aquifer system and the thickness of the unsaturated zone. Thus, large-scale climate oscillations such as the NAO, are likely to affect recharge rates and mechanisms in aquifers across the UK, which is a response that has previously been identified in the High Plains aquifer of the United States (Gurdak et al. 2007). Additional factors related to the aquifer (Slimani et al. 2009) or observation point (borehole) may also be important such as its proximity to rivers, for example if river stage locally influences groundwater levels where there is good groundwater/surface-water connection (Luque-Espinar et al. 2008). Although the water levels at the three boreholes used in this study are not affected by abstraction, the spatiotemporal patterns of groundwater abstraction in other more heavily exploited aquifers may present a substantial complexity in identifying and interpreting the effects of climate variability and change on groundwater levels (Gurdak et al 2007).

The analyses presented have demonstrated the value of wavelet methods in identifying the synchronization of groundwater-level dynamics by climate variability at multiannual, decadal, or longer time scales. That wavelet methods can show that groundwater-level dynamics in spatially disparate and hydrogeologically separate aquifers are entrained by environmental correlation, with teleconnections between recurrent and persistent climatic patterns over large parts of the Earth's surface, is of great societal importance in the context of climate change (Post and Forchhammer 2002) and reinforces the need for hydrogeologists to make increasing use of such methods which do not assume stationarity.

Acknowledgements We acknowledge the British Geological Survey for provision of the groundwater level data. John Bloomfield publishes with the permission of the Executive Director, British Geological Survey (NERC). We thank Aslak Grinsted for making his wavelet coherence package freely available.

References

- Allen DJ, Brewerton LJ, Coleby LM, Gibbs BR, Lewis MA, MacDonald AM, Wagstaff SJ, Williams AT (1997) The physical properties of major aquifers in England and Wales. British Geological Survey Technical Report WD/97/34, BGS, Keyworth, UK
- Barker PA, Wilby RL, Borrows J (2004) A 200-year precipitation index for the central English Lake District. *Hydrol Sci J* 49:769–785
- Blackburn M, Hoskins B (2001) The UK record-breaking wet Autumn 2000. UK Univ Global Atmos Modell Prog Newslett 24
- Boggess A, Narcowich FJ (2001) A first course in wavelets with Fourier analysis. Prentice Hall, New York
- Carmona R, Hwang WL, Torresani B (1998) Practical time frequency analysis, vol 9: Gabor and wavelet transforms with an implementation in S (Wavelet analysis and its applications). Academic, San Diego
- CPC (Climate Prediction Centre) (2010) Northern Hemisphere Teleconnection Patterns.

CPC, Camp Springs, MD. <http://www.cpc.noaa.gov/data/teledoc/telecontents.shtml>. Cited 20 July 2010

CRU (Climatic Research Unit) (2010) North Atlantic Oscillation (NAO). CRU, Norwich, UK. <http://www.cru.uea.ac.uk/cru/data/nao/>. Cited 20 July 2010

Dickinson JE, Hanson RT, Ferre TPA et al (2004) Inferring time varying recharge from inverse analysis of long-term water levels. *Water Resour Res* 40. doi:10.1029/2003WR002650, 15 p

Enfield DB, Mestas-Nuñez AM, Trimble PJ (2001) The Atlantic multidecadal oscillation and its relation to rainfall and river flows in the continental U.S. *Geophys Res Lett* 28 (10):2077–2080

Farge M (1992) Wavelet transform and their application to turbulence. *Ann Rev Fluid Mech* 24:395–457

Ghil M, Allen RM, Dettinger MD, Ide K, Kondrashov D, Mann ME, Robertson A, Saunders A, Tian Y, Varadi F, Yiou P (2002) Advanced spectral methods for climatic time series. *Rev Geophys* 40(1):3.1–3.41

Grinsted A, Moore JC, Jevrejeva S (2004) Application of the cross wavelet transform and wavelet coherence to geophysical time series. *Nonlinear Proc Geophys* 11:561–566

Grinsted A, Moore JC, Jevrejeva S (2011) Cross wavelet and wavelet coherence. <http://www.pol.ac.uk/home/research/waveletcoherence/>. Cited 22 May 2011

Gurdak JJ, Hanson RT, McMahon PB et al (2007) Climate variability controls on unsaturated water and chemical movement, High Plains Aquifer, USA. *Vadose Zone J* 6:533–547

Gurdak JJ, Hanson RT, Green RT (2009) Effects of climate variability and change on groundwater resources of the United States. *US Geol Surv Fact Sheet* 2009–3074, 4 pp

Hannaford J, Marsh TJ (2008) High-flow and flood trends in a network of undisturbed catchments in, the UK. *Int J Climat* 28:1325–1338

Hanson RT, Newhouse MW, Dettinger MD (2004) A methodology to assess relations between climatic variability and variations in hydrologic time series in the southwestern United States. *J Hydrol* 287(1–4):252–269

Hanson RT, Dettinger MD, Newhouse MW (2006) Relations between climatic variability and hydrologic time series from four alluvial basins across the southwestern United States. *Hydrogeol J* 14(7):1122–1146

Henderson RD, Day-Lewis FD, Harvey CF (2009) Investigation of aquifer–estuary interaction using wavelet analysis of fiber-optic temperature data. *Geophys Res Lett* 36:L06403. doi:10.1029/2008GL036926

Holman IP, Rivas-Casado M, Howden NJK, Bloomfield JP, Williams AT (2009) Linking North Atlantic ocean-atmosphere teleconnection patterns and hydrogeological responses in temperate groundwater systems. *Hydrol Proc* 23:3123–3126

Hurrell JW (1995) Decadal trends in the North Atlantic Oscillation: regional temperatures and precipitation. *Science* 269:676–679

Jones IC, Banner JL (2003) Hydrogeologic and climatic influences on spatial and interannual, variation of recharge to a tropical karst island aquifer. *Water Resour Res* 39(9). doi:10.1029/2002WR001543

- Jones PD, Jonsson T, Wheeler D (1997) Extension to the North Atlantic Oscillation using early instrumental pressure observations from Gibraltar and south-west Iceland. *Int J Climatol* 17:1433–1450
- Luque-Espinar JA, Chica-Olmo M, Pardo-Iguzquiza E, Garcia-Soldado MJ (2008) Influence of climatological cycles on hydraulic heads across a Spanish Aquifer. *J Hydrol* 354:33–52
- Mantua NJ, Hare SR (2002) The Pacific decadal oscillation. *J Oceanog* 58(1):35–44
- Maraun D, Kurths J (2004) Cross wavelet analysis: significance testing and pitfalls. *Nonlinear Proc Geophys* 11:505–514
- Marsh TJ, Hannaford J (2008) UK Hydrometric Register. Hydrological data UK series. Centre for Ecology and Hydrology, Wallingford, UK, 210 pp
- Meyer Y (1993) Wavelets and applications. Society for Industrial and Applied Mathematics, Philadelphia, PA
- Milly PCD, Betancourt J, Falkenmark M, Hirsch RM, Kundzewicz ZW, Lettenmaier DP, Stouffer RJ (2008) Stationarity is dead: Whither water management? *Science* 319:573–574
- Nason GP (2008) Wavelet methods in statistics with R. Springer, Heidelberg, Germany
- Osborn TJ (2006) Recent variations in the winter North Atlantic Oscillation. *Weather* 61(12):353–355
- Percival DB, Walden AT (2000) Wavelet methods for time series analysis. Cambridge University Press, Cambridge
- Post E, Forchhammer MC (2002) Synchronization of animal population dynamics by large-scale climate. *Nature* 420 (6912):168–171
- Price M (1993) The Chalk as an aquifer. In: Downing RA, Price M, Jones GP (eds) *The hydrogeology of the Chalk of North-West Europe*. Oxford Science, Oxford, UK, pp 35–58
- Qian BD, Saunders MA (2003) Summer UK temperature and its links to preceding Eurasian snow cover, North Atlantic SSTs, and the NAO. *J Clim* 16:4108–4120
- Schroder TM, Rosbjerg D (2004) Groundwater recharge and capillary rise in a clayey catchment: modulation by topography and the Arctic Oscillation. *Hydrol Earth Syst Sci* 8:1090–1102
- Slimani S, Massei N, Mesquita J et al (2009) Combined climatic and geological forcings on the spatio-temporal variability of piezometric levels in the chalk aquifer of Upper Normandy (France) at pluridecennial scale. *Hydrogeol J* 17:1823–1832
- Stephenson DB, Pavan V, Collins M, Junge MM et al (2006) North Atlantic Oscillation response to transient greenhouse gas forcing and the impact on European winter climate: a CMIP2 multi-model assessment. *Clim Dyn* 27:401–420
- Torrence C, Compo PG (1997) A practical guide to wavelet analysis. *Bull Am Meteorol Soc* 79(1):61–78
- Walnut DF (2002) *An introduction to wavelet analysis*. Birkhauser, Basel, Switzerland

Figures

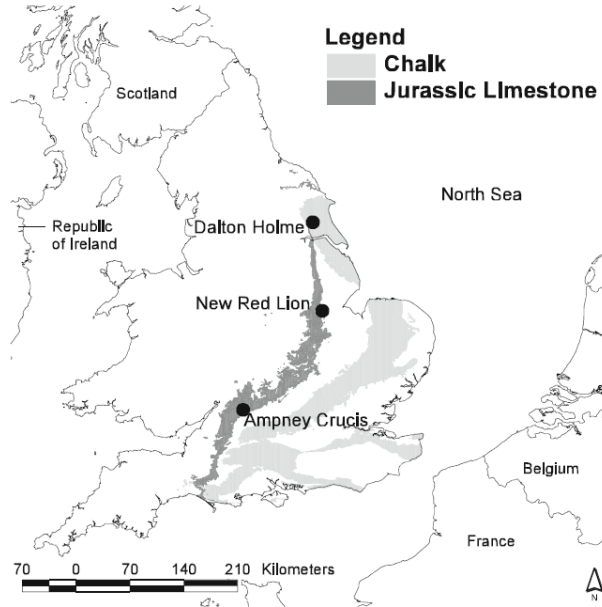


Figure 1. Location of the studied boreholes and aquifers in England

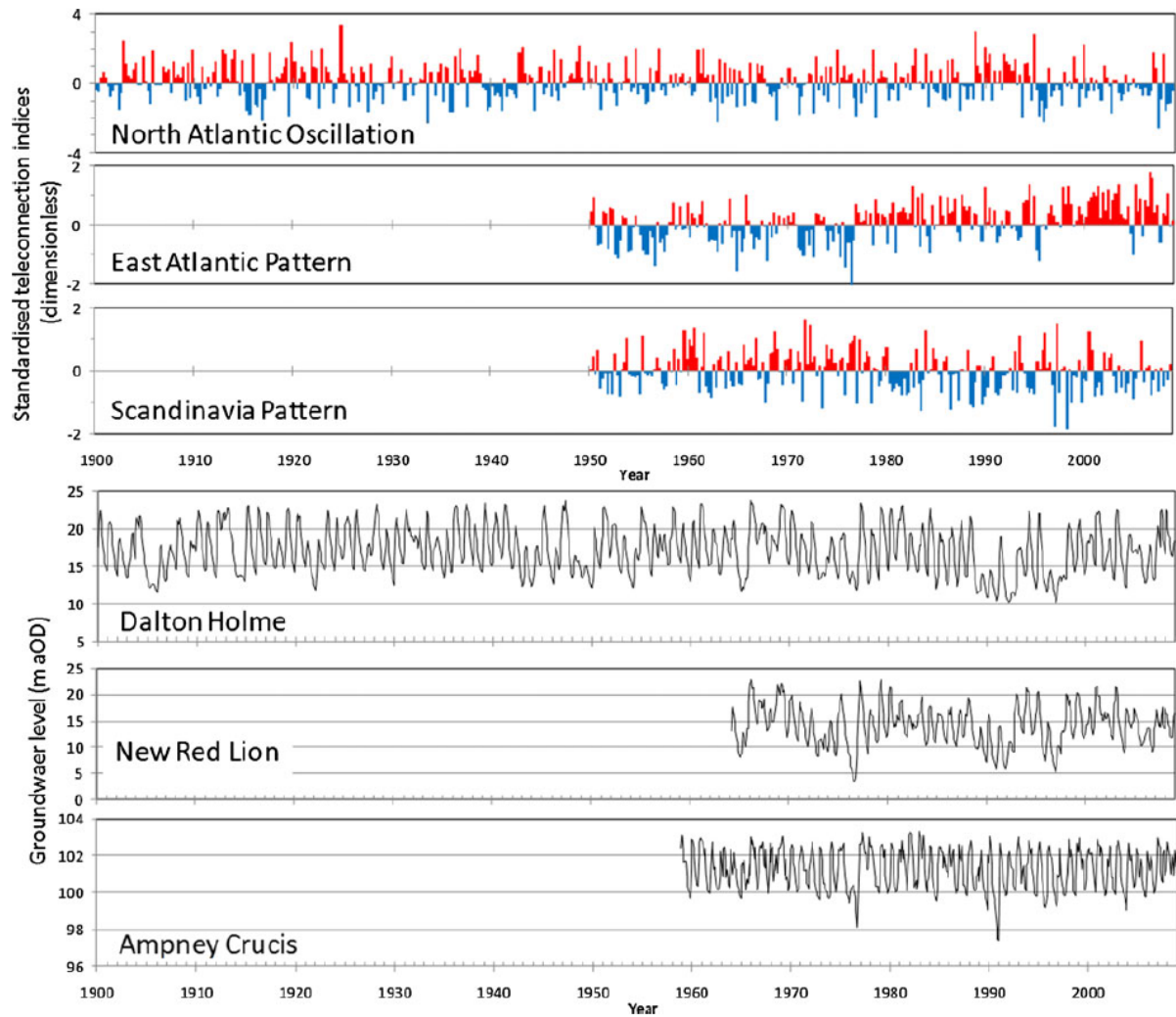


Figure 2. Positive (red) and negative (blue) phases of the standardised seasonal teleconnection indices and monthly groundwater levels (NAO data from the Climatic Research Unit; other climate data from the Climate Prediction Centre)

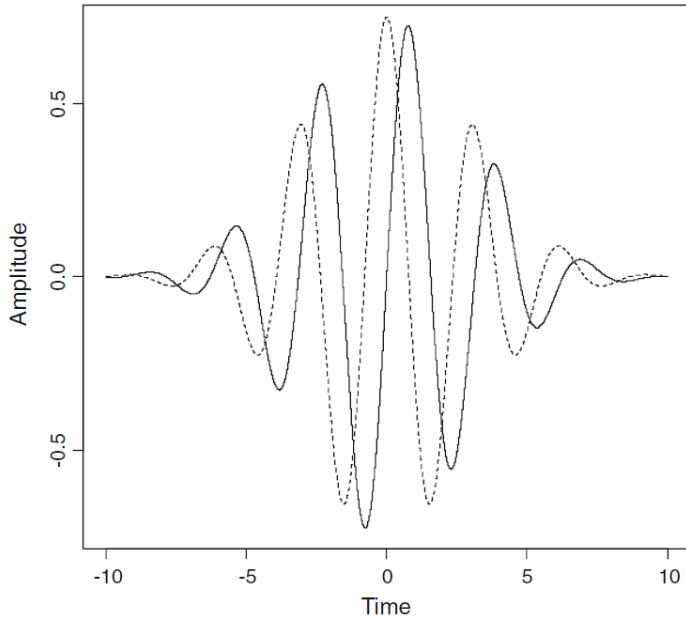


Figure 3. Real (dashed line) and imaginary (solid line) parts of the Morlet wavelet with $\omega = 6$ (units are arbitrary)

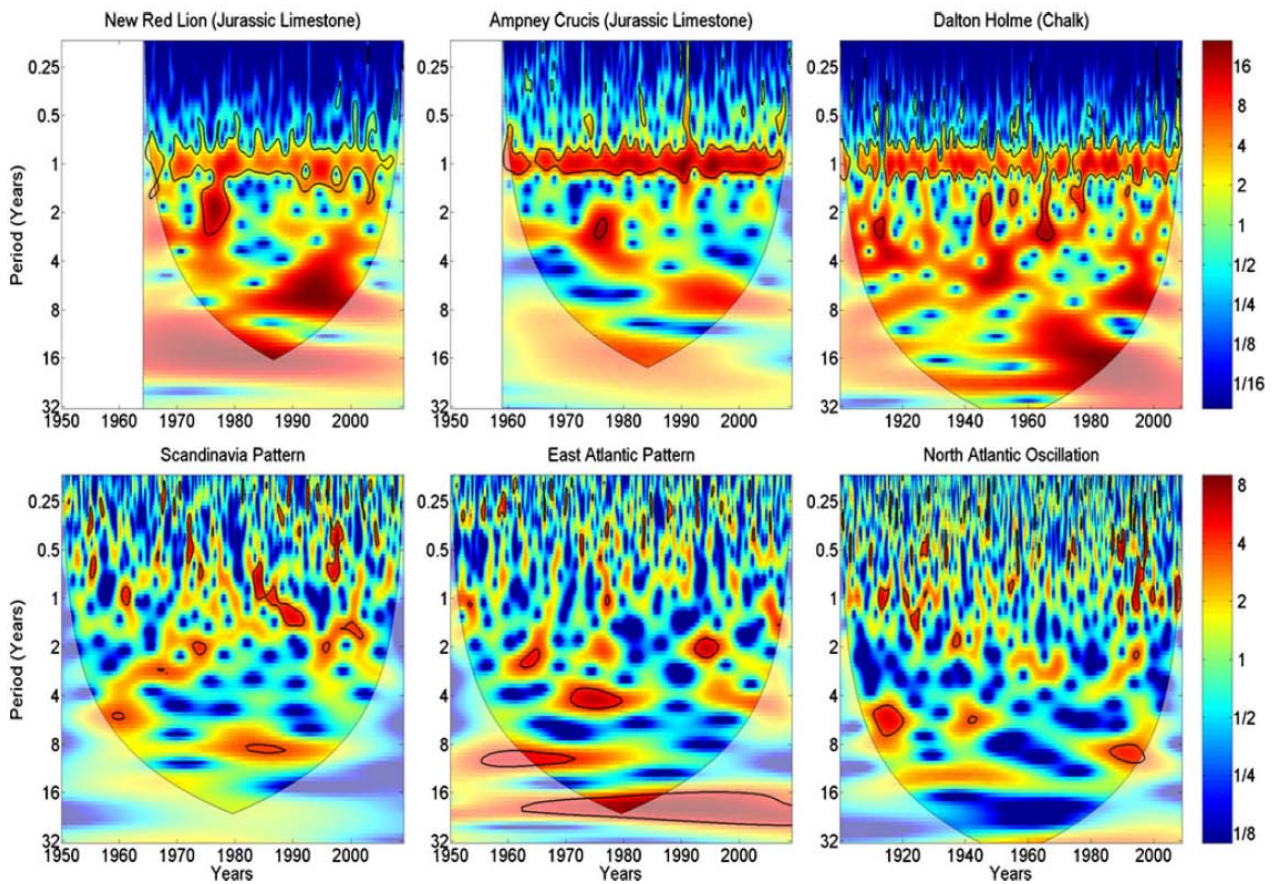


Figure 4. The CWT spectra of (upper row) groundwater levels (at New Red Lion, Ampney Crucis and Dalton Holme) and (lower row) Scandinavia Pattern, East Atlantic Pattern and the North Atlantic Oscillation teleconnection indices (note that spectral power is dimensionless and the longer timescales for the CWT spectrum at Dalton Holme and NAO as there are much longer historic data sets for NAO and groundwater levels at this site)

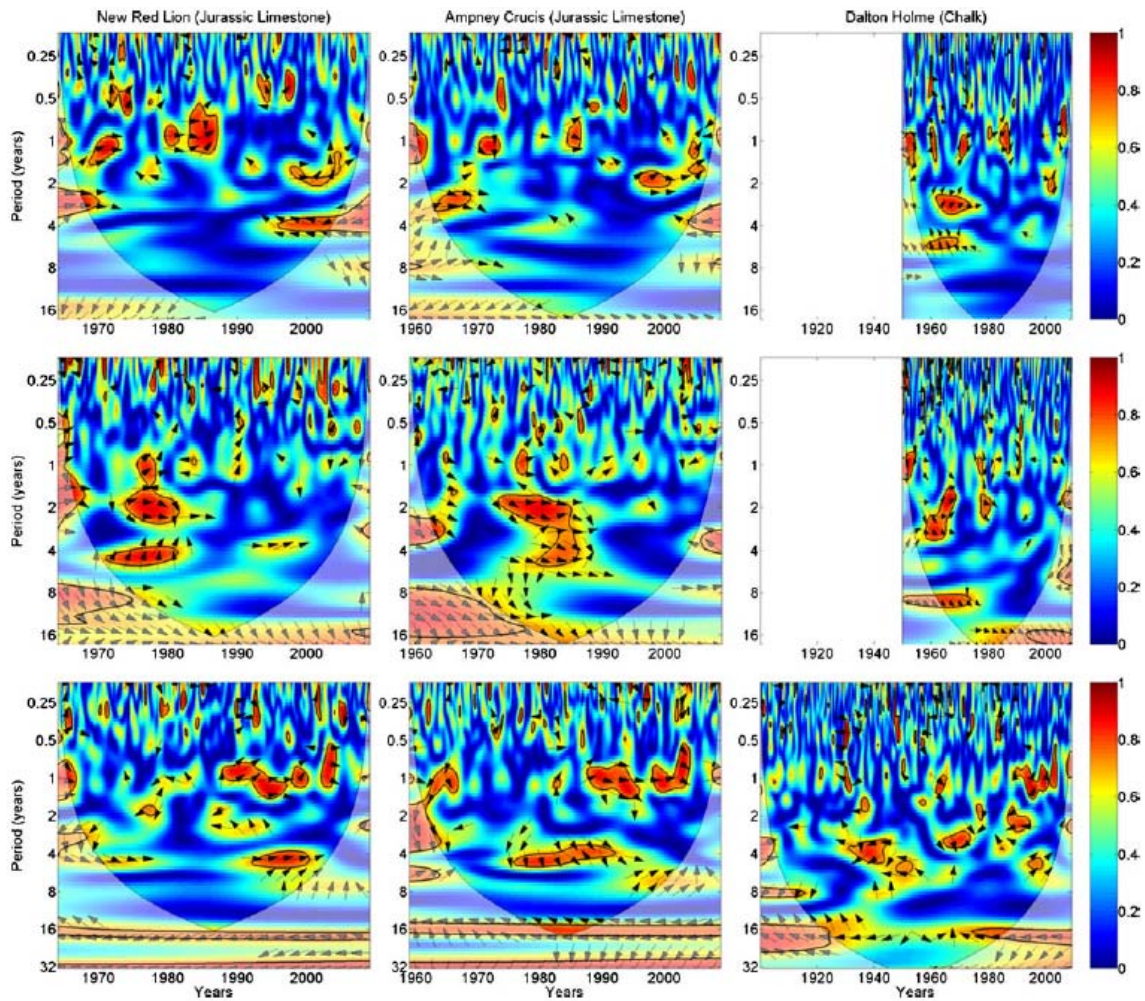


Figure 5. Wavelet coherence between groundwater levels at New Red Lion, Crucis Ampney and Dalton Holme (vertical panels), and North Atlantic teleconnection indices of the (upper row) East Atlantic Pattern, (middle row) Scandinavia Pattern, and the (lower row) North Atlantic Oscillation. Note that spectral power is dimensionless, the thick black lines are the 5% significance level, and the less intense colours denote the COI. The vectors indicate the phase difference between the data; a horizontal arrow pointing from left to right signifies in phase and an arrow pointing vertically upward means the groundwater level series lags the teleconnection index by 90° (i.e., the phase angle is 270°)

Tables

Borehole	Data period	Mean depth to groundwater (m)	Mean groundwater level (m aOD)	Groundwater level range (m aOD)	Groundwater fluctuation (m)	Autocorrelation (months)
Ampney Crucis	12/1958–02/2009	8.26	101.26	97.41 to 103.25	5.84	8
New Red Lion	03/1964–02/2009	19.39	14.06	3.37 to 23.35	19.98	6
Dalton Holme	01/1900–02/2009	17.38	17.12	10.19 to 23.76	13.57	10

aOD above ordnance datum \equiv mean sea level

Table 1 Summary of features of the three hydrographs used in the study